Int. J. Heat Mass Transfer. Vol. 32, No. 7, pp. 1373–1376, 1989
Printed in Great Britain

0017–9310/89 $3.00+0.00
Maxwell Pergamon Macmillan plc

TECHNICAL NOTES

Melt propagation in porous media

SUDIP S. DOSANJH
Reactor Safety Theoretical Physics Division, 6425, Sandia National Laboratories, Albuquerque, NM 87185, U.S.A.

(*Received* 5 *October* 1988 *and in final form* 8 *December* 1988)

INTRODUCTION

DURING severe nuclear reactor accidents similar to Three-Mile Island, the fuel rods can fragment and thus convert the reactor core into a large porous bed composed primarily of UO_2 and ZrO_2 particles [1]. As energy is released by fission product decay, liquid coolant in the bed can boil away and temperatures can eventually surpass the UO_2–ZrO_2 melting point (2800 K) [2]. Of interest to this study are heat transfer and melt propagation in the bed after the particles become dry (here, dry refers to the absence of liquid coolant).

Several researchers [3–8] have studied phase change phenomena in porous media. Ogniewicz and Tien [3], Huang [4] and others [5–7] investigated liquid/gas phase changes in systems containing three phases (solid, liquid and gas). More recently, Beckermann and Viskanta [8] studied solid/liquid phase changes when only two phases are present. In the present work solid/liquid phase changes are of interest and three phases are present simultaneously. Only a limited amount of qualitative information is available in this area [9].

The work presented in this note is an extension of a recently developed one-dimensional model of melt propagation in porous media [2]. This note discusses a two-dimensional model that considers the melting of a porous solid and the subsequent refreezing of the melt in colder portions of the bed as the liquid relocates under the action of gravity and capillary forces. The effects of varying the particle diameter, composition and bed height are also discussed.

ANALYSIS

Formulation

The following assumptions are employed.

(1) The average particle diameter, d_p, is taken to be much smaller than the distance characteristic of macroscopic changes in temperature and species concentrations, x_c. Therefore, the microscopic governing equations can be volume averaged to yield macroscopic porous medium equations.

(2) A modified version of Darcy's law that accounts for the presence of three phases can be used [10].

(3) Movement of the gas has a negligible effect on the motion of the melt and heat transfer—gas velocities are usually low, of the order of 1 cm s^{-1} [2].

(4) Radiation heat transfer through the bed can be modeled using a temperature-dependent thermal conductivity.

(5) The solid and the liquid are in local thermal equilibrium.

(6) On the particle scale, the species are well mixed and the UO_2–ZrO_2 phase diagram given by Hagrman [11] can be used. This implies that $d_p \ll [D\tau_c]^{1/2}$, where D is a diffusion coefficient and τ_c is the time scale of interest (e.g. the time associated with the heat-up of the bed). Further, species diffusion is neglected over length scales comparable to the characteristic distance x_c—that is, $[D\tau_c]^{1/2} \ll x_c$. In summary, $d_p \ll [D\tau_c]^{1/2} \ll x_c$.

(7) Properties remain fixed at constant values.

In addition, it is assumed that the particles remain fixed in space as they melt. This assumption is clearly not valid at extremely high porosities. However, scoping experiments [9] conducted in a research reactor indicate that the particles do not start settling downward until the porosity surpasses a value of about 0.7. As the solid melts, some fraction of the liquid is trapped near the contact points between particles by surface tension forces. These surface tension forces also tend to hold the particles in place. When the particles eventually start moving, the analysis presented in this note breaks down and consequently, results presented here are only valid until the porosity reaches a value of 0.7.

Using these assumptions the model consists of the following equations.

Conservation of mass

$$\frac{\partial}{\partial t}[Y_{\ell j}\rho_{\ell j}\varepsilon S]+\nabla\cdot[Y_{\ell j}\rho_{\ell j}\mathbf{u}] = -\frac{\partial}{\partial t}[Y_{sj}\rho_{sj}(1-\varepsilon)] \quad (1)$$

for each species j ($j = 1$ for UO_2 and $j = 2$ for ZrO_2). The Y_{lj} are related to each other by $Y_{\ell 1}+Y_{\ell 2} = 1$ and $Y_{s1}+Y_{s2} = 1$.

Conservation of momentum

$$\frac{\mu}{\kappa_\ell}\mathbf{u} = -\nabla P_\ell - \mathbf{g}\rho_\ell. \quad (2)$$

Equation (2) is similar to the traditional form of Darcy's law: the only difference is that the permeability κ defined in Bird *et al.* [12] is replaced by a relative permeability κ_ℓ to account for the presence of three phases (solid, liquid and gas). Typically, κ_ℓ depends on the particle diameter, d_p, the porosity, ε, the saturation, S, and a critical value of the saturation, S_r, that is often referred to as the residual saturation [13]. The quantity S_r is defined as the threshold value of saturation below which bulk liquid motion ceases. For $S \leqslant S_r$, $\kappa_\ell = 0$ and equation (2) requires that $\mathbf{u} = 0$. When the saturation is less than the critical value, the liquid is trapped between the particles by surface tension effects [13]. Liquid starts to flow when the saturation is increased to the point that these pockets of trapped liquid touch and coalesce [13]. At the other extreme, as the saturation approaches 1, κ_ℓ approaches κ. That is, when $S = 1$, only two phases are present (solid and liquid) and the relative permeability must equal the permeability for the flow of a single fluid through a porous matrix.

Capillary forces enter equation (2) through the term involving the liquid pressure, P_ℓ. The capillary pressure is defined as the difference between P_ℓ and the gas pressure, P_g (that is, $P_c = P_g - P_\ell$) [10, 13]. This difference arises because of surface tension effects: that is, the capillary pressure is

NOMENCLATURE

c_p	specific heat [J kg^{-1} K^{-1}]
d_p	particle diameter [mm]
D	mass diffusivity [m^2 s^{-1}]
g	gravitational acceleration [m s^{-2}]
h	enthalpy [J kg^{-1}]
h_f	heat of fusion [J kg^{-1}]
J	Leverett function
k	thermal conductivity [W m^{-1} K^{-1}]
L	bed height [m]
P_c	capillary pressure [N m^{-2}]
P_g	gas pressure [N m^{-2}]
P_ℓ	liquid pressure [N m^{-2}]
Q	decay heat [W kg^{-1} of UO_2]
r	radial distance [m]
S	saturation (fraction of porosity ε occupied by liquid)
S_e	effective saturation, $(S-S_r)/(1-S_r)$
S_r	residual saturation (value of S below which liquid motion ceases)
t	time [s]
T	temperature [K]
u	superficial liquid velocity [m s^{-1}]
x	distance from the bottom of the bed [m]
$Y_{\ell j}$	(volume of liquid species j)/(volume of liquid)
Y_{sj}	(volume of solid species j)/(volume of solid).

Greek symbols

α_i	volume fraction of phase i
α_{eff}	thermal diffusivity [m^2 s^{-1}]
γ	surface tension [N m^{-1}]
ε	porosity (liquid and gas volume fraction, $\alpha_\ell+\alpha_g$)
ε_r	emissivity
κ	permeability [m^2]
κ_ℓ	relative permeability [m^2]
μ	viscosity [Pa s]
ρ	theoretical density [kg m^{-3}]

Subscripts

g	gas
i	phase
j	species ($j=1$ for UO_2 and $j=2$ for ZrO_2)
ℓ	liquid
s	solid.

zero in systems of zero surface tension. In the applications of interest, gas velocities are low, the gas pressure changes by a small amount and the pressure gradient term in equation (2) can be replaced using $\nabla P_\ell = -\nabla P_c$. From equation (2) it is therefore evident that capillary forces move liquid into regions of high P_c. Using dimensional analysis, Leverett [13] concluded that the capillary pressure is given by $P_c = J\gamma(\varepsilon/\kappa)^{1/2}$, where γ is the surface tension and J is an empirically determined function of the effective saturation, $S_e = (S-S_r)/(1-S_r)$. As the particle diameter increases, κ increases [12] and P_c decreases—consequently, capillary forces are small in beds with large particles. Decreasing ε increases both ε/κ [12] and P_c and consequently, capillary forces tend to move liquid into regions of lower porosity. This behavior is similar to the classical capillarity demonstration discussed by Batchelor [14] in which liquid is observed to rise in a small diameter tube when the tube is inserted into an infinite liquid pool.

Conservation of energy

$$\frac{\partial}{\partial t}\sum_j[(1-\varepsilon)Y_{sj}\rho_{sj}h_{sj}+\varepsilon SY_{\ell j}\rho_{\ell j}h_{\ell j}]+\nabla\cdot\sum_j \mathbf{u}Y_{\ell j}\rho_{\ell j}h_{\ell j}$$
$$=\nabla\cdot k_{eff}\nabla T+[(1-\varepsilon)\rho_{s1}Y_{s1}+\varepsilon S\rho_{\ell 1}Y_{\ell 1}]Q. \quad (3)$$

Closure

Correlations for κ, κ_ℓ, S_r, J and k_{eff} are given in the Appendix. In order to solve this set of equations, the decay heat, properties, a phase diagram, enthalpies, as well as initial and boundary conditions must be specified. Typically, the decay heat, Q, is of the order of 300 W kg^{-1} of UO_2 and the maximum value of the ZrO_2 volume fraction, Y_{s2}, is 0.36 [2]. Typical UO_2 and ZrO_2 properties are given in Table 1. The viscosity, μ, of the melt is 0.005 Pa s and the surface tension, γ, is 0.45 N m^{-1} [11].

The UO_2–ZrO_2 phase diagram given by Hagrman [11] is used (UO_2–ZrO_2 mixtures start melting at 2800 K over a wide range of compositions). If we assume that the specific heat of each species j is constant, then $h_{sj} = c_{pj}(T-T_{ref})$ and $h_{\ell j} = c_{pj}(T-T_{ref})+h_{fj}$.

Initially, uniform porosity and composition profiles are prescribed and the temperature is set to 1500 K. The outside boundaries continue to radiate to an environment at 1500 K as temperatures in the bed increase. On the centerline, the radial component of the velocity is set equal to 0 and the radial derivative of temperature ($\partial T/\partial r$) is also set equal to 0.

Solution algorithm

Equations (1) and (3) are solved using a computational cell method [15] in which temperatures and species volume fractions are determined at the centers of the cells and velocities are calculated at the sides. A time-explicit finite difference scheme is employed and the convective terms in equations (1) and (3) are calculated using central differencing. Typically, 200 computational cells are needed to resolve temperature and species gradients in the bed.

ORDER OF MAGNITUDE ANALYSIS

Consider a debris bed with an initial temperature, T_0, where T_0 is less than the melting temperature. If the boundaries radiate to cold environments as temperatures in the bed increase, then boundary information becomes important over the entire domain at time $t = L^2/\alpha_{eff}$, where α_{eff} is an average thermal diffusivity and L is the height of the bed (in the problems of interest to this study, the radial extent of the bed is of the same order as L). Using the properties in Table 1, setting $\varepsilon = 0.4$, $k_{eff} = 5$ W m^{-1} K^{-1} and $L = 1$ m gives: $\alpha_{eff} \simeq k_{eff}/[(1-\varepsilon)\rho_s c_{ps}] \simeq 10^{-6}$ m^2 s^{-1} and $L^2/\alpha_{eff} \simeq 10^6$ s. For the times of interest, conduction is only important within boundary layers of thickness $\delta \simeq [\alpha_{eff}t]^{1/2}$. In the center of the bed, temperatures increase approximately linearly with time until the solid starts melting.

Table 1. Typical UO_2 and ZrO_2 properties [11]

Property	UO_2	ZrO_2
Solid density, ρ_{sj} [kg m^{-3}]	10000	5700
Liquid density, $\rho_{\ell j}$ [kg m^{-3}]	9000	5700
Specific heat, c_{pj} [J kg^{-1} K^{-1}]	630	700
Thermal conductivity, k_j [W m^{-1} K^{-1}]	3.0	2.0
Heat of fusion, h_{fj} [kJ kg^{-1}]	274	706

RESULTS AND DISCUSSION

Base case

Calculations are presented in this section for a 0.5 m high, 0.5 m diameter particle bed with a ZrO_2 : UO_2 mass ratio of 0.1, which corresponds to a ZrO_2 volume fraction of 0.15, an initial porosity of 0.4 and an average particle diameter of 1 mm. The effects of varying the particle diameter, the bed height and the composition are discussed in subsequent sections.

Temperature contours at 3400 s are shown in Fig. 1. Note that the 2800 K contour approximates the boundary of the melt zone. Solid first melts at 3100 s, increasing the porosity in the center of the bed and decreasing the local solid volume fraction, α_s. The melt subsequently relocates under the action of both gravity and capillary forces. Capillary forces, which tend to move liquid into regions of lower porosity, induce liquid out of the melt zone in a roughly symmetric manner. A downward velocity due to gravity is superimposed on this capillary motion.

Solid volume fractions at 3800 s are shown in Fig. 2. Note that as melt relocates it refreezes in colder regions near the boundaries of the bed. Dense refrozen regions with $\alpha_s > 0.6$ form when the melt reaches the thermal boundary layer. Most of the melt flows downward, creating the dark region with $\alpha_s > 0.8$ in Fig. 2. However, a small fraction of the melt flows upward and radially outward. After the formation of the $\alpha_s > 0.8$ region in Fig. 2, the model predicts the creation of a molten pool similar to the one found at Three-Mile Island [1] as liquid accumulates above this blockage.

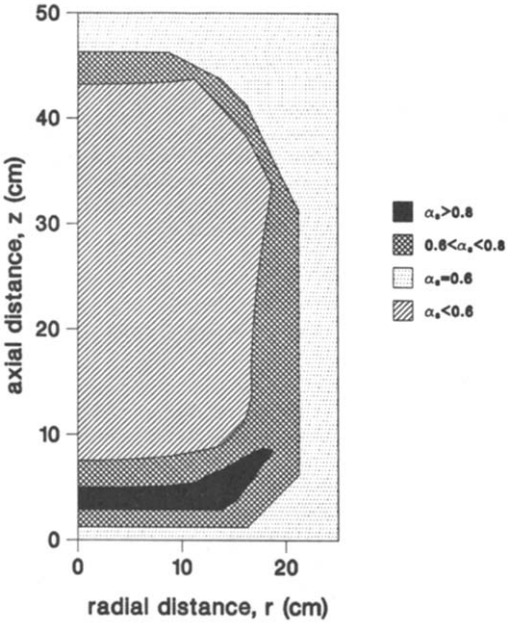

FIG. 2. Solid volume fraction (α_s) profiles at 3800 s in a bed with 1 mm diameter particles. The bed has an initial uniform volume fraction of 0.6.

Sensitivity analysis

Particle diameter. Solutions were also obtained for a bed with 5 mm diameter particles—all other parameters were held fixed at their base case values. As evidenced by Fig. 3, the melt zone is smaller and the refrozen regions form closer to the center in a bed with larger particles. Raising d_p enhances radiation heat transfer in the bed (the radiative contribution to the effective conductivity is proportional to d_p), thus increasing the thermal boundary layer thickness, δ.

It is also worth noting that the capillary pressure is inversely proportional to d_p ($P_c \sim 1/\kappa^{1/2}$ and $\kappa \sim d_p^2$). Thus, capillary forces become less important, compared to gravity, as the particle diameter is increased. Note that a refrozen region with $\alpha_s > 0.6$ has not formed above the melt zone in Fig. 3 (such a region is evident in Fig. 2).

Initial composition. Zirconia : urania mass ratios of 0.1, 0.2 and 0.3, corresponding to initial ZrO_2 volume fractions of 0.15, 0.25 and 0.35, respectively, were considered. Decreasing the UO_2 concentration reduces the decay heating and melt formation is delayed by several hundred seconds as the ZrO_2 : UO_2 mass ratio increases from 0.1 to 0.3. On the other hand, flow characteristics remained relatively unaffected. After initial melt formation, approximately 100 s elapsed

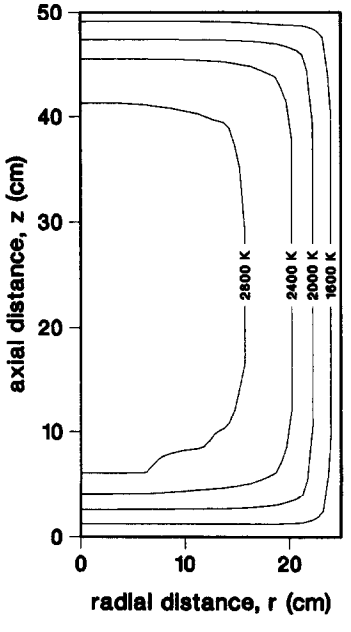

FIG. 1. Temperature contours at 3400 s in a bed with 1 mm diameter particles.

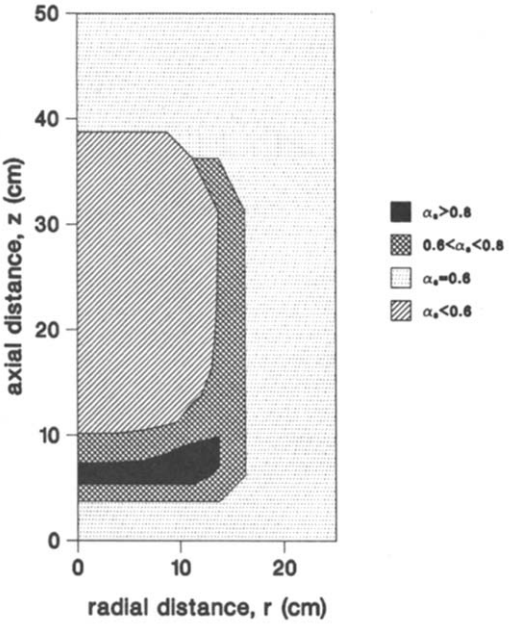

FIG. 3. Solid volume fraction (α_s) profiles at 3800 s in a bed with 5 mm diameter particles. The bed has an initial uniform volume fraction of 0.6.

before macroscopic liquid motion was evident and a refrozen region started forming 300 s later in all three cases.

Bed height. Three bed heights were considered: 0.50, 0.75 and 1.00 m. As one would expect, the timing of initial melt formation was independent of the bed height, L. Furthermore, the refrozen regions formed at the same locations (relative to the boundaries of the bed) in each calculation because the thermal boundary layer thickness is also independent of L. Consequently, the size of the melt zone increased approximately linearly with L.

CONCLUSIONS

Key results are that (1) when solid starts melting, the liquid relocates under the action of gravity and capillary forces, refreezing upon reaching colder regions near the boundaries of the bed; (2) a flow blockage forms near the bottom of the bed and the location of this blockage is determined primarily by the bottom thermal boundary layer thickness; (3) increasing the particle diameter increases the radiative contribution to the effective conductivity, raising the thermal boundary layer thickness and consequently, reducing the size of the melt zone; (4) decreasing the UO_2 concentration reduces the amount of energy released by fission product decay and delays melting by several hundred seconds; and (5) the size of the melt zone increases linearly with the height of the bed.

Acknowledgements—This work was supported by the United States Nuclear Regulatory Commission and was performed at Sandia National Laboratories, which is operated for the U.S. Department of Energy under contract number DE-AC04-76DP00789.

REFERENCES

1. E. L. Tolman, TMI-2 Accident Scenario Update, EGG-TMI-7489, Idaho National Engineering Laboratory, Idaho Falls, Idaho (1986).
2. S. S. Dosanjh, Melting and refreezing of porous media, *Int. J. Heat Fluid Flow* (1989), in press.
3. Y. Ogniewicz and C. L. Tien, Analysis of condensation in porous insulation, *Int. J. Heat Mass Transfer* **24,** 421–429 (1981).
4. C. L. D. Huang, Multi-phase moisture transfer in porous media subjected to temperature gradient, *Int. J. Heat Mass Transfer* **22,** 1295–1307 (1979).
5. S. B. Nasrallah and P. Perre, Detailed study of a model of heat and mass transfer during convective drying of porous media, *Int. J. Heat Mass Transfer* **31,** 957–967 (1988).
6. O. A. Plumb, G. A. Spolek and B. A. Olmstead, Heat and mass transfer in wood during drying, *Int. J. Heat Mass Transfer* **28,** 1669–1678 (1985).
7. S. Motakef and M. A. El-Masri, Simultaneous heat and mass transfer with phase change in porous slab, *Int. J. Heat Mass Transfer* **29,** 1503–1512 (1986).
8. C. Beckermann and R. Viskanta, Natural convection solid/liquid phase change in porous media, *Int. J. Heat Mass Transfer* **31,** 35–46 (1988).
9. J. T. Hitchcock and J. E. Kelly, Post-test examinations of the in-pile molten pool experiments, *Trans. Am. Nucl. Soc.* **43,** 515 (1982).
10. A. E. Scheidegger, *The Physics of Flow Through Porous Media* (3rd Edn), pp. 266–290. University of Toronto Press, Toronto (1974).
11. D. L. Hagrman, *MATPRO—Version 11 (Revision 2): A Handbook of Material Properties for Use in the Analysis of Light Water Reactor Fuel Rod Behavior*, NUREG/CR-0479. Idaho National Engineering Laboratory, Idaho Falls, Idaho (1981).
12. R. B. Bird, W. E. Stewart and E. N. Lightfoot, *Transport Phenomena* (1st Edn), p. 199. Wiley, New York (1960).
13. M. C. Leverett, Capillary behavior in porous solids, *Pet. Trans. AIME* **142,** 152–169 (1941).
14. G. K. Batchelor, *An Introduction to Fluid Dynamics* (1st Edn), p. 67. Cambridge University Press, Cambridge (1967).
15. S. V. Patankar, *Numerical Heat Transfer and Fluid Flow* (1st Edn). McGraw-Hill, New York (1980).

APPENDIX. PHYSICAL CHARACTERISTICS

Bird *et al.* [12] derived the following equation for the permeability:

$$\kappa = \frac{d_p^2 \varepsilon^3}{150(1-\varepsilon)^2}. \tag{A1}$$

The relative permeability, κ_ℓ, is given by [2]: $\kappa_\ell = \kappa S_e^3$ for $S > S_r$ and $\kappa_\ell = 0$ for $S \leqslant S_r$. The residual saturation, S_r, is given by [2]:

$$S_r = \frac{1}{86.3}\left[\frac{\gamma}{\kappa \rho_\ell g}\right]^{0.263} \tag{A2}$$

The following relation gives the Leverett function, J [2]: $J = a(S_e + B)^{-c}$, where $a = 0.38$, $b = 0.014$ and $c = 0.27$.

The following correlation gives k_{eff} [2]:

$$k_{eff} = \psi k_g^* + \frac{1-\psi}{k_\sigma w + k_g^*(1-w)} k_\sigma k_g^* \tag{A3}$$

where k_σ is the average thermal conductivity of the solid and the liquid, $w = 0.3\phi^{1.6}(k_\sigma/k_g^*)^{-0.044}$, $\psi = (\phi - w)/(1-w)$ and $\phi\,(\equiv \varepsilon - \varepsilon S)$ is the volume fraction occupied by gas. Radiation heat transfer in the bed is incorporated using a modified gas conductivity, $k_g^* = k_g + k_{rad}$, where $k_{rad} = 4\varepsilon_r \sigma d_p T^3$.